Organic−Inorganic Perovskites Containing Trivalent Metal Halide Layers: The Templating Influence of the Organic Cation Layer

David B. Mitzi

IBM T. J. Watson Research Center, P.O. Box 218, Yorktown Heights, New York 10598

Received July 17, 2000

Thin sheetlike crystals of the metal-deficient perovskites $(H_2AEQT)M_{2/3}I_4$ [M = Bi or Sb; AEQT = 5,5‴-bis-(aminoethyl)-2,2′:5′,2″:5″,2‴-quaterthiophene] were formed from slowly cooled ethylene glycol/2-butanol solutions containing the bismuth(III) or antimony(III) iodide and AEQT·2HI salts. Each structure was refined in a monoclinic (*C*2/*m*) subcell, with the lattice parameters $a = 39.712(13)$ Å, $b = 5.976(2)$ Å, $c = 6.043(2)$ Å, $\beta = 92.238(5)°$, and $Z = 2$ for M = Bi and $a = 39.439(7)$ Å, $b = 5.952(1)$ Å, $c = 6.031(1)$ Å, $\beta = 92.245(3)°$, and $Z = 2$ for M = Sb. The trivalent metal cations locally adopt a distorted octahedral coordination, with M−I bond lengths ranging from 3.046(1) to 3.218(3) Å (3.114 Å average) for M = Bi and 3.012(1) to 3.153(2) Å (3.073 Å average) for M = Sb. The new organic−inorganic hybrids are the first members of a metal-deficient perovskite family consisting of $(M^{n+})_{2/n}V_{(n-2)/n}X_4^{2-}$ sheets, where V represents a vacancy (generally left out of the formula) and the metal cation valence, *n*, is greater than 2. The organic layers in the AEQT-based organic−inorganic hybrids feature edge-to-face aromatic interactions among the rigid, rodlike quaterthiophene moieties, which may help to stabilize the unusual metal-deficient layered structures.

Introduction

The organic−inorganic perovskite family has yielded a remarkable degree of structural versatility.[1] In the $(R-NH_3)_2(CH_3NH_3)_{n-1}M_nX_{3n+1}$ and $(H_3N-R-NH_3)(CH_3NH_3)_{n-1}M_nX_{3n+1}$ series (R = organic group, M = divalent metal, X = halide), for example, the crystal structures consist of "*n*"-layer-thick ⟨100⟩-oriented slabs, cut from the three-dimensional $CH_3NH_3MX_3$ perovskite structure, interleaved with organic bilayers (i.e., for monoammonium cations) or monolayers (i.e. for diammonium cations).[2,3] Increasing "*n*" leads to a transition from two-dimensional to a more three-dimensional inorganic framework. A wide range of organic R groups can be incorporated in the ⟨100⟩-oriented family, including many alkyl and simple aromatic components. Interestingly, certain organic cations favor the formation of a distinct family of ⟨110⟩-oriented perovskites.[4] In the $[NH_2C(I)=NH_2]_2(CH_3NH_3)_nM_nX_{3n+2}$ (M = divalent metal, X = halide) series, for example, one- ($n = 1$), two- ($n \geq 2$), and three-dimensional ($n \rightarrow \infty$) ⟨110⟩-oriented frameworks can all be stabilized within a single structural family.[5] In this series, the iodoformamidinium cation templates the formation of the unusual perovskite framework. Selected other organic cations (besides iodoformamidinium) have been shown to stabilize the ⟨110⟩-oriented perovskite structures.[6,7]

In addition to structural flexibility, interesting physical properties arise in the organic−inorganic perovskite hybrids as a result of the unusual structural attributes. For certain combinations of organic and inorganic constituents the hybrids can be considered self-assembling quantum well structures, with semiconducting inorganic sheets alternating with wider band gap organic layers. The tin(II) iodide based $(C_4H_9NH_3)_2(CH_3NH_3)_{n-1}Sn_nI_{3n+1}$ and $[NH_2C(I)=NH_2]_2(CH_3NH_3)_nSn_nI_{3n+2}$ compounds, for example, exhibit a large electrical mobility and a semiconductor−metal transition as a function of increasing perovskite sheet thickness (controlled by "*n*").[2,4,8] A field-effect transistor, based on a spin-coated organic−inorganic tin(II) iodide based perovskite channel layer, has recently been demonstrated with a field-effect mobility of 0.6 $cm^2/V·s$.[9]

Perovskites based on group IVA metal halide sheets and optically inert organic cations also exhibit sharp, tunable resonances in their room-temperature optical absorption and emission spectra, arising from exciton states associated with the band gap of the metal halide framework.[10] In these systems, the organic component of the structure generally consists of alkylammonium or single ring aromatic ammonium cations and the organic HOMO−LUMO energy gap is large compared to the band gap of the inorganic framework. Recently, dye-based cations have also been substituted into the layered perovskite framework, with HOMO−LUMO gaps comparable to or smaller than the inorganic framework band gap.[1,11−13] The chromophore molecules have a substantial impact on the optical properties

(1) For a recent review, see: Mitzi, D. B. *Prog. Inorg. Chem.* **1999**, *48*, 1.
(2) Mitzi, D. B.; Feild, C. A.; Harrison, W. T. A.; Guloy, A. M. *Nature* **1994**, *369*, 467.
(3) Calabrese, J.; Jones, N. L.; Harlow, R. L.; Herron, N.; Thorn, D. L.; Wang, Y. *J. Am. Chem. Soc.* **1991**, *113*, 2328.
(4) Mitzi, D. B.; Wang, S.; Feild, C. A.; Chess, C. A.; Guloy, A. M. *Science* **1995**, *267*, 1473.
(5) Wang, S.; Mitzi, D. B.; Feild, C. A.; Guloy, A. *J. Am. Chem. Soc.* **1995**, *117*, 5297.
(6) Mitzi, D. B.; Liang, K.; Wang, S. *Inorg. Chem.* **1998**, *37*, 321.
(7) Mousdis, G. A.; Gionis, V.; Papavassiliou, G. C.; Raptopoulou, C. P.; Terzis, A. *J. Mater. Chem.* **1998**, *8*, 2259.
(8) (a) Mitzi, D. B.; Feild, C. A.; Schlesinger, Z.; Laibowitz, R. B. *J. Solid State Chem.* **1995**, *114*, 159. (b) Mitzi, D. B.; Liang, K. *J. Solid State Chem.* **1997**, *134*, 376.
(9) Kagan, C. R.; Mitzi, D. B.; Dimitrakopoulos, C. D. *Science* **1999**, *286*, 945.
(10) Ishihara, T. In *Optical Properties of Low-Dimensional Materials*; Ogawa, T., Kanemitsu, Y., Eds.; World Scientific: Singapore, 1995; pp 288−339.
(11) Mitzi, D. B.; Chondroudis, K.; Kagan, C. R. *Inorg. Chem.* **1999**, *38*, 6246.
(12) Era, M.; Maeda, K.; Tsutsui, T. *Chem. Phys. Lett.* **1998**, *296*, 417.
(13) Braun, M.; Tuffentsammer, W.; Wachtel, H.; Wolf, H. C. *Chem. Phys. Lett.* **1999**, *303*, 157.

10.1021/ic000794i CCC: $19.00
Published on Web 11/30/2000

of these hybrids and can lead to strongly luminescent materials. Bright room-temperature electroluminescence has been observed from a hybrid perovskite based on a lead(II) chloride framework and the quaterthiophene derivative, 5,5‴-bis(aminoethyl)-2,2′:5′,2″:5″,2‴-quaterthiophene (AEQT).[14]

While great flexibility has been demonstrated with regard to substitutions within the organic layers of hybrid perovskite structures, the flexibility of the inorganic framework has been limited by the need to incorporate divalent metals. This valency requirement derives from the need to balance charge between the organic cation and the metal halide anion layers. In the single layer (i.e., $n = 1$) ⟨100⟩-oriented perovskites, $(NH_3-R-NH_3)MX_4$, for example, the MX_4^{2-} perovskite sheets counterbalance the $NH_3-R-NH_3^{2+}$ layers. With X = Cl^-, Br^-, or I^-, "M" must be a divalent cation that can adopt an octahedral coordination (e.g., Cu^{2+}, Mn^{2+}, Co^{2+}, Cd^{2+}, Ge^{2+}, Sn^{2+}, Pb^{2+}, Eu^{2+}).[1] The ability to incorporate non-divalent metal cations within the organic−inorganic perovskite framework would enhance the possibility of identifying inorganic frameworks with new and useful (e.g., semiconducting, ferroelectric, optical, magnetic) properties.

In principle, the metal site, "M", might be expected to accommodate an equal proportion of trivalent and monovalent cations (still therefore providing the correct average 2+ charge) or, for higher-valent (> 2+) systems, a mixture of metal cations and vacancies. Mixed cation systems (with mixed valency) are well established for strictly inorganic three-dimensional perovskites based on metal oxide frameworks [e.g., $Ba(Bi_{0.5}Nb_{0.5})O_3$].[15] However, among the organic−inorganic metal halide based perovskites, less flexibility has been reported. In an effort to identify examples of layered organic−inorganic perovskites that do not consist of divalent metal halide perovskite sheets, as well as to search for new systems that contain semiconducting inorganic frameworks, we began to consider systems containing trivalent metals. In this contribution, layered bismuth(III) and antimony(III) halide based perovskite structures are demonstrated, stabilized by vacancy formation on the metal site and an appropriate choice of organic cation (the quaterthiophene derivative H_2AEQT^{2+}).

It should be noted that the formation of single layers of corner-sharing metal halide octahedra is unusual in bismuth(III) and antimony(III) hybrid chemistry. As for conventional perovskite frameworks, bismuth(III) and antimony(III) halide lattices generally consist of distorted MX_6 octahedra. These MX_6 octahedra form discrete (i.e., mononuclear) or extended (i.e., polynuclear) inorganic networks of corner-, edge-, or face-sharing octahedra, leading to an extensive family of metal(III) halogenoanions (e.g., MX_4^-, MX_5^{2-}, MX_6^{3-}, $M_2X_9^{3-}$, $M_2X_{11}^{5-}$, $M_3X_{12}^{3-}$, $M_4X_{18}^{6-}$, $M_5X_{18}^{3-}$, $M_6X_{22}^{4-}$, and $M_8X_{30}^{6-}$).[16] Within these networks, the metal(III) sites are essentially fully occupied. Despite the numerous examples of organic−inorganic bismuth and antimony iodide hybrids, there are few, if any, known examples of ⟨100⟩-oriented perovskite structures analogous to the $(R-NH_3)_2MX_4$ and $(H_3N-R-NH_3)MX_4$ compounds (M = divalent metal cation). Therefore, in addition to considering the basic crystal structures and properties of the new trivalent-metal-containing hybrid perovskite family, this study also addresses the potential role played by the rigid quaterthiophene molecule in stabilizing the metal-deficient perovskite sheets.

Experimental Section

Synthesis. Crystals of $(H_2AEQT)M_{2/3}I_4$ (M = Bi and Sb) were grown from slowly cooled, saturated, ethylene glycol/2-butanol solutions containing the corresponding organic and inorganic salts. The synthesis of AEQT·2HI has been previously described.[11] The BiI_3 and SbI_3 salts (Aldrich, 99.999%, anhydrous) were purified by sublimation. For M = Bi, equimolar quantities of AEQT·2HI (161.4 mg; 0.24 mmol) and BiI_3 (141.5 mg; 0.24 mmol) were weighed and added to a test tube under an inert atmosphere. The contents completely dissolved at 112 °C in a solvent mixture of 36 mL of ethylene glycol (Aldrich, anhydrous, 99.8%) and 0.6 mL of concentrated (57 wt %) aqueous HI (Aldrich, stabilized, 99.99%). Upon gradual addition of 18 mL of 2-butanol (Aldrich, anhydrous, 99.5%), a small amount of red precipitate began to form. Heating the mixture to 116 °C in the sealed tube led to the precipitate going back into solution. Subsequent slow cooling of the solution at 1.5 °C/h to −20 °C produced a high yield (220 mg; 0.21 mmol) of dark red, sheetlike crystals of the $(H_2AEQT)Bi_{2/3}I_4$ compound. Note that 2-butanol was added to the solution to enhance the temperature dependence of the solubility of the product. When no 2-butanol was added, the yield was substantially lower upon cooling (although the same product formed). Chemical analysis of the product was consistent with the proposed $C_{20}H_{22}S_4N_2Bi_{2/3}I_4$ formula; theoretical [found]: C 22.54 [22.6], H 2.08 [2.2], N 2.63 [2.5], S 12.04 [12.1].

Crystals of the analogous M = Sb compound were also prepared from a slightly acidified ethylene glycol/2-butanol solution, as described above for the M = Bi compound. The color and morphology of the $(H_2AEQT)Sb_{2/3}I_4$ crystals were similar to those observed for the bismuth analogue, as was the powder X-ray diffraction pattern [with only (*h*00) reflections observed in the highly oriented crystalline deposits].

X-ray Crystallography. A very thin, sheetlike $(H_2AEQT)Bi_{2/3}I_4$ [$(H_2AEQT)Sb_{2/3}I_4$] crystal, with the approximate dimensions ∼0.005 mm × 0.12 mm × 0.27 mm [<0.01 mm × 0.06 mm × 0.24 mm], was selected under a microscope and attached to the end of a quartz fiber with 5 min epoxy. A full sphere of data was collected at room temperature using a Bruker SMART CCD diffractometer, equipped with a normal focus 2.4 kW sealed tube X-ray source (Mo Kα radiation, λ = 0.71073 Å). Intensity data were collected with a detector distance of approximately 5.0 cm, in 2272 frames with increasing ω, and an exposure time of 200 s [240 s] per frame. The increment in ω between each frame was 0.3°. Note that while the final crystals chosen (as well as other candidates examined) were well formed in two dimensions, the third dimension was very thin, leading to problems with weak diffraction and crystal warping. The rocking curves for the reflections were substantially broadened compared to more typical, well-behaved (i.e., thicker) crystals from other systems.

Both structures can be successfully refined either in a *C*2/*m* subcell or in a *C*2/*c* cell with doubled *c* axis. The latter cell is isostructural with that recently reported for $(H_2AEQT)PbX_4$.[11] In the current structures, the strongest and most well-defined set of diffraction peaks correspond to the subcell with lattice parameters (*C*2/*m* space group) a = 39.712(13) Å, b = 5.976(2) Å, c = 6.043(2) Å, β = 92.238(5)° [for M = Bi] and a = 39.439(7) Å, b = 5.952(1) Å, c = 6.031(1) Å, β = 92.245(3)° [for M = Sb]. As for the $(H_2AEQT)PbX_4$ structures,[11] there are reflections that double the cell along the *c* axis. In contrast to the lead(II) systems, however, the supercell reflections for the trivalent-metal-containing systems are weak, somewhat broad, and relatively few in number, especially for the antimony(III) compound. The lack of intensity of these reflections may derive from the quality of the crystals or from the existence of vacancies within the metal halide sheets, which might reduce the degree of perfection of the ordering that gives rise to the superstructure. As a result of the substantially better refinement results for the smaller cell [i.e., for M = Bi, R_f = 0.076, R_w = 0.078, GOF = 2.83 (*C*2/*m* subcell) versus R_f = 0.083, R_w = 0.093, GOF = 3.05 (*C*2/*c* cell); for M = Sb, R_f = 0.062, R_w = 0.068, GOF = 2.17 (*C*2/*m* subcell) versus R_f = 0.078, R_w = 0.093, GOF = 3.11 (*C*2/*c* cell)], the subcell results are primarily discussed in the current manuscript. For comparison, the *C*2/*c* cell data are given in the Supporting Information. Finally, as for the lead(II) systems, there are also features in the CCD frames that correspond to a further superstructure, doubling the unit cell along both the *a* and *c* axes. While

(14) Chondroudis, K.; Mitzi, D. B. *Chem. Mater.* **1999**, *11*, 3028.
(15) Galasso, F. S. *Structure, Properties and Preparation of Perovskite-Type Compounds*; Pergamon Press: New York, 1969.
(16) Fisher, G. A.; Norman, N. C. *Adv. Inorg. Chem.* **1994**, *41*, 233.

Table 1. Crystallographic Data for $(H_2AEQT)Bi_{2/3}I_4$ and $(H_2AEQT)Sb_{2/3}I_4$

chemical formula	$C_{20}H_{22}S_4N_2Bi_{2/3}I_4$	$C_{20}H_{22}S_4N_2Sb_{2/3}I_4$
fw	1065.61	1007.46
space group	*C*2/*m* (No. 12)	*C*2/*m* (No. 12)
a, Å	39.712(13)	39.439(7)
b, Å	5.976(2)	5.952(1)
c, Å	6.043(2)	6.031(1)
β, deg	92.238(5)	92.245(3)
V, Å^3	1432.9(8)	1414.6(5)
Z	2	2
ρ_{calcd}, g/cm^3	2.470	2.366
wavelength (Å)	0.71073 (Mo Kα)	0.71073 (Mo Kα)
abs coeff (μ), cm^{-1}	87.25	53.41
R_f[a]	0.076	0.062
R_w[b]	0.078	0.068

[a] $R_f = \sum(|F_o| - |F_c|)/\sum(|F_o|)$. [b] $R_w = \{\sum w(|F_o| - |F_c|)^2/\sum(w|F_o|^2)\}^{1/2}$.

a number of these superstructure features are strong, the reflections exhibit very broad, streaklike rocking curves, suggesting a poorly ordered superstructure.[11] The diffuse reflections are neglected in the current structural model and discussion.

The final cell parameters and crystal orientation matrix were obtained by a least-squares fit of 8192 reflections. An empirical absorption correction, based on equivalent reflections, was applied to the intensity data.[17] The structure was solved and refined using the NRCVAX 386 PC version program.[18] First, the Bi [Sb] and I atoms were located using direct methods. The S, N, and C atoms were then located using successive Fourier difference maps. All non-hydrogen atoms were refined anisotropically. Given the limitations on the data quality imposed by the very thin and slightly warped crystals, no effort was made to locate the hydrogen atoms. The occupancy of the Bi [Sb] site was refined to 0.67[0.64]. Initial attempts to refine the occupancy of the other heavy atoms did not lead to values substantially different from unity (or one-half for disordered sites). Therefore, these occupancies were held fixed during the final refinement. The minimum and maximum peaks in the final difference Fourier map corresponded to −1.30 and 4.62 e/Å^3 [−1.00 and 2.66 e/Å^3], with the first three residual peaks appearing within 2 Å of either Bi [Sb] or I. No additional symmetry was detected using the MISSYM program.[19] Selected crystallographic results for both compounds are summarized in Table 1. The atomic coordinates for $(H_2AEQT)Bi_{2/3}I_4$ and $(H_2AEQT)Sb_{2/3}I_4$ are listed in Tables 2 and 3, respectively. Selected bond distances and angles are provided for each compound in Tables 4 and 5. A complete listing of crystallographic data and bond distances and angles, along with anisotropic displacement parameters for each compound, are given as Supporting Information.

Results and Discussion

Crystal Structure. Bismuth(III)/antimony(III) halide structures generally consist of distorted MX_6 octahedra, which share corners, edges, or faces to form discrete or extended inorganic networks. Among the bismuth iodides, isolated BiI_6 octahedra are found in $(C_6H_5CH_2CH_2NH_3)_4BiI_7 \cdot H_2O$,[20] with iodide anions and water molecules interposed between the octahedra in the inorganic layers of the structure. Chains of corner-sharing octahedra are found in $(H_3NC_6H_{12}NH_3)BiI_5$,[21] as well as in analogous BiI_5^{2-} systems containing the longer and more complex organic molecules 1,6-bis[5′-(2″-aminoethyl)-2′-thienyl]hexane (AETH) and 1,12-dodecanediamine (DDDA).[22] In (2-picolinium)BiI_4 and (quinolinium)BiI_4, the polymeric inorganic anion is constructed from edge-sharing BiI_6 octahedra,[23,24] while in $(Ph_4P)_3Bi_5I_{18}$, the anion consists of a linear chain of five face-sharing octahedra.[25] Other examples of bismuth(III)

Table 2. Positional and Thermal Parameters[a] for $(H_2AEQT)Bi_{2/3}I_4$

atom	*x*	*y*	*z*	B_{iso} (Å^2)
Bi	0.0	0.0	0.0	3.4(2)
I(1)	0.08109(7)	0.0	0.0101(4)	5.2(2)
I(2)[b]	0.0	0.0973(7)	0.5	3.8(2)
I(3)[b]	−0.0008(1)	0.5	0.0980(7)	3.9(2)
S(1)	0.1585(3)	0.5	−0.145(2)	6.3(7)
S(2)[b]	0.2108(4)	0.379(3)	0.267(2)	5.4(7)
N(1a)[b]	0.068(2)	0.5	−0.33(1)	6(2)
N(1b)[c]	0.069(2)	0.33(1)	−0.49(1)	4(2)
C(1a)[b]	0.080(3)	0.5	−0.57(2)	7(4)
C(1b)[b]	0.082(3)	0.5	−0.48(2)	7(3)
C(2a)[b]	0.119(3)	0.5	−0.57(2)	7(3)
C(2b)[c]	0.118(4)	0.41(2)	−0.50(2)	5(3)
C(3)[b]	0.140(2)	0.403(9)	−0.412(9)	6(1)
C(4)[b]	0.154(1)	0.201(7)	−0.476(7)	3(1)
C(5)[b]	0.178(1)	0.101(8)	−0.334(8)	5(1)
C(6)[b]	0.182(1)	0.228(8)	−0.126(8)	4(1)
C(7)[b]	0.204(1)	0.177(8)	0.059(8)	4(1)
C(8)	0.223(1)	0.0	0.091(7)	5.6(9)
C(9)	0.243(1)	0.0	0.282(6)	5.0(9)
C(10)[b]	0.241(1)	0.217(9)	0.408(7)	4(1)

[a] The heavy atoms (Bi, I, and S) are refined anisotropically; anisotropic thermal parameters are listed in Table S2 (Supporting Information). [b] Occupancy = 1/2. [c] Occupancy = 1/4.

Table 3. Positional and Thermal Parameters[a] for $(H_2AEQT)Sb_{2/3}I_4$

atom	*x*	*y*	*z*	B_{iso} (Å^2)
Sb	0.0	0.0	0.0	3.6(2)
I(1)	0.07999(5)	0.0	0.0074(3)	5.6(1)
I(2)[b]	0.0	0.0794(5)	0.5	4.5(2)
I(3)[b]	−0.0012(1)	0.5	0.0765(5)	4.6(2)
S(1)	0.1585(2)	0.5	0.851(1)	5.4(4)
S(2)[b]	0.2110(2)	0.379(2)	0.266(2)	4.6(4)
N(1a)[b]	0.069(1)	0.5	0.664(7)	4.9(9)
N(1b)[c]	0.069(1)	0.33(1)	0.507(9)	5(1)
C(1a)[b]	0.079(4)	0.5	0.45(2)	8(4)
C(1b)[b]	0.083(2)	0.5	0.50(1)	8(2)
C(2a)[b]	0.118(2)	0.5	0.41(2)	9(3)
C(2b)[c]	0.118(2)	0.42(1)	0.48(1)	3(2)
C(3)[b]	0.1401(9)	0.405(5)	0.583(5)	4.7(8)
C(4)[b]	0.1523(9)	0.210(7)	0.531(6)	5.4(9)
C(5)[b]	0.1758(7)	0.092(5)	0.670(5)	3.3(6)
C(6)[b]	0.1812(8)	0.224(6)	0.877(5)	4.0(7)
C(7)[b]	0.2038(7)	0.179(5)	0.061(5)	3.4(6)
C(8)	0.2225(7)	0.0	0.098(4)	4.8(6)
C(9)	0.2434(6)	0.0	0.282(4)	3.8(5)
C(10)[b]	0.2415(8)	0.204(6)	0.409(5)	4.0(7)

[a] The heavy atoms (Sb, I, and S) are refined anisotropically; anisotropic thermal parameters are listed in Table S3 (Supporting Information). [b] Occupancy = 1/2. [c] Occupancy = 1/4.

Table 4. Selected Bond Distances (Å) and Angles (deg) for $(H_2AEQT)Bi_{2/3}I_4$

Bi−I(1)	3.218(3)	I(1)[a]−Bi−I(2)[b]	91.13(4)
Bi−I(1)[a]	3.218(3)	I(1)[a]−Bi−I(2)[c]	88.87(4)
Bi−I(2)[b]	3.077(1)	I(1)[a]−Bi−I(3)	89.2(1)
Bi−I(2)[c]	3.077(1)	I(1)[a]−Bi−I(3)[a]	90.8(1)
Bi−I(3)	3.046(1)	I(2)[b]−Bi−I(3)	90.3(1)
Bi−I(3)[a]	3.046(1)	I(2)[b]−Bi−I(3)[a]	89.7(1)
I(1)−Bi−I(1)[a]	180.0	I(2)[c]−Bi−I(3)	89.7(1)
I(1)−Bi−I(2)[b]	88.87(4)	I(2)[c]−Bi−I(3)[a]	90.3(1)
I(1)−Bi−I(2)[c]	91.13(4)	I(3)−Bi−I(3)[a]	180.0
I(1)−Bi−I(3)	90.8(1)	Bi−I(2)[b]−Bi[b]	158.2(2)
I(1)−Bi−I(3)[a]	89.2(1)	Bi−I(3)−Bi[d]	157.5(2)

[a] $-x, -y, -z$. [b] $x, y, -1 + z$. [c] $-x, -y, 1 - z$. [d] $x, 1 + y, z$.

(17) Sheldrick, G. M. *SADABS*; Institut für Anorganische Chemie der Universität Göttingen: Göttingen, 1997.
(18) Gabe, E. J.; Le Page, Y.; Charland, J.-P.; Lee, F. L.; White, P. S. *J. Appl. Crystallogr.* **1989**, *22*, 384.
(19) Le Page, Y. *J. Appl. Crystallogr.* **1988**, *21*, 983.
(20) Papavassiliou, G. C.; Koutselas, I. B.; Terzis, A.; Raptopoulou, C. P. *Z. Naturforsch.* **1995**, *50b*, 1566.
(21) Mousdis G. A.; Papavassiliou, G. C.; Terzis, A.; Raptopoulou, C. P., *Z. Naturforsch.* **1998**, *53b*, 927.
(22) Mitzi, D. B.; Brock, P. *Inorg. Chem.*, submitted.

Table 5. Selected Bond Distances (Å) and Angles (deg) for $(H_2AEQT)Sb_{2/3}I_4$

Sb−I(1)	3.153(2)	I(1)[a]−Sb−I(2)[b]	91.42(3)
Sb−I(1)[a]	3.153(2)	I(1)[a]−Sb−I(2)[c]	88.58(3)
Sb−I(2)[b]	3.0522(7)	I(1)[a]−Sb−I(3)	88.87(9)
Sb−I(2)[c]	3.0522(7)	I(1)[a]−Sb−I(3)[a]	91.13(9)
Sb−I(3)	3.0123(7)	I(2)[b]−Sb−I(3)	89.94(8)
Sb−I(3)[a]	3.0123(7)	I(2)[b]−Sb−I(3)[a]	90.06(8)
I(1)−Sb−I(1)[a]	180.0	I(2)[c]−Sb−I(3)	90.06(8)
I(1)−Sb−I(2)[b]	88.58(3)	I(2)[c]−Sb−I(3)[a]	89.94(8)
I(1)−Sb−I(2)[c]	91.42(3)	I(3)−Sb−I(3)[a]	180.0
I(1)−Sb−I(3)	91.13(9)	Sb−I(2)[b]−Sb[b]	162.2(1)
I(1)−Sb−I(3)[a]	88.87(9)	Sb−I(3)−Sb[d]	162.2(1)

[a] $-x, -y, -z$. [b] $x, y, -1 + z$. [c] $-x, -y, 1 - z$. [d] $x, 1 + y, z$.

halide frameworks include the $Bi_2I_9^{3-}$ compounds, which generally consist of isolated pairs of face-sharing BiI_6 octahedra.[26,27] A similar range of structures has also been found for the corresponding antimony(III) iodides.[16,21,25]

Among the bismuth(III) and antimony(III) iodides, there is currently a lack of examples of ⟨100⟩-oriented layered hybrid perovskites. Such systems would require vacancies on the metal sites within the inorganic sheets to satisfy valency requirements. Attempts to stabilize this structural type using bismuth(III) iodide and various long, relatively flexible, organic cations, such as diprotonated AETH and DDDA, led to the formation of a distinct class of hybrids containing chains of corner-sharing bismuth(III) iodide octahedra.[22] These reactions were carried out in ethylene glycol/2-butanol or hydriodic acid solutions, respectively, and the appropriate organic and inorganic salts were dissolved in a 1:1 molar ratio. Using similar reaction conditions and replacing the relatively flexible moieties with a more rigid AEQT molecule resulted in single-phase formation of crystals with the structure shown in Figure 1.

The inorganic framework of $(H_2AEQT)Bi_{2/3}I_4$ consists of $Bi_{2/3}I_4^{2-}$ metal-deficient perovskite sheets separated by layers of the organic cation. Each bismuth(III) atom is surrounded by a distorted octahedral coordination of iodides (see Table 4), with bond lengths ranging from 3.046(1) to 3.218(3) Å [3.114 Å average]. Both bridging iodides in the subcell model, I(2) and I(3), are refined as disordered over two symmetry-related sites, with occupancy fixed at 0.5. In contrast, both the bismuth(III) atom and the terminal iodide, I(1), are not disordered. Adjacent BiI_6 octahedra share four corners to form the inorganic sheets (Figure 2). The structure and disordering of the inorganic sheets is very similar to that recently discussed for $(H_2AEQT)PbX_4$ (X = Br, I).[11] However, in the lead(II) systems, the metal sites are fully occupied. During the structural refinement of the bismuth(III) compound, the occupancy of the bismuth site refined to $\sim^2/_3$, thereby confirming the stoichiometry (as determined from chemical analysis) and the presence of apparently randomly distributed vacancies on the metal site. The inorganic framework for the antimony(III) hybrid structure is very similar to that discussed for the bismuth(III) analogue, with Sb−I bond lengths (Table 5) ranging from 3.012(1) to 3.153(2) Å [3.073 Å average].

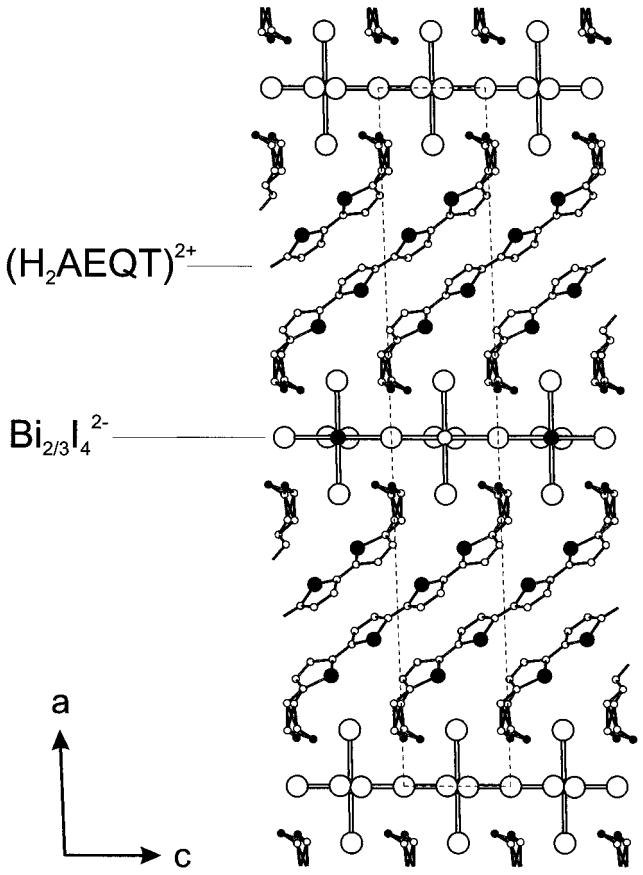

Figure 1. Crystal structure (*C*2/*m* cell) of $(H_2AEQT)Bi_{2/3}I_4$, viewed down the *b* axis. The dashed lines show the unit cell outline. For clarity, the atoms are represented as spheres with uniform sizes selected for each atom type. Small black (filled) and white (unfilled) spheres represent occupied and unoccupied bismuth(III) sites, respectively, within the $Bi_{2/3}I_4^{2-}$ sheets. The metal-site vacancies occur randomly within the bismuth iodide layers.

Among the trivalent group VA compounds, several perovskite-like structures have been previously reported. In $Cs_3Bi_2Br_9$, a trigonal structure results, with double layers of corner-sharing octahedra.[28] The resulting framework is similar to that of the cubic perovskite, $CsPbBr_3$, with, however, one-third of the metal sites vacant. The same structure is also formed for $(CH_3NH_3)_3Bi_2Br_9$.[29] In contrast to the title compounds, the vacancies in these systems are ordered, yielding a structure which can be considered a double-layer version of a ⟨111⟩-oriented perovskite (as opposed to a single-layer ⟨100⟩-oriented system).[30] Within the $Bi_2Br_9^{3-}$ double layers, the metal sites are fully occupied. The countercation, which balances the bismuth(III) bromide anion, is also very simple (either a large inorganic cation or a very small organic cation). For more complex organic cations, the bismuth(III) bromide layers generally break down into isolated $Bi_2Br_9^{3-}$ clusters.[31] Similarly, the corresponding iodide structures, $Cs_3Bi_2I_9$ and $(CH_3NH_3)_3Bi_2I_9$, revert to isolated $Bi_2I_9^{3-}$ anions composed of two face-sharing BiI_6 octahedra.[32,33]

(23) Robertson, B. K.; McPherson, W. G.; Meyers, E. A. *J. Phys. Chem.* **1967**, *71*, 3531.
(24) Nagapetyan, S. S.; Arakelova, A. R.; Ziger, E. A.; Koshkin, V. M.; Struchkov, Y. T.; Shklover, V. E. *Russ. J. Inorg. Chem.* **1989**, *34*, 1276.
(25) Pohl, S.; Peters, M.; Haase, D.; Saak, W. *Z. Naturforsch.* **1994**, *49b*, 741.
(26) Lazarini, F. *Acta Crystallogr.* **1987**, *C43*, 875.
(27) Gridunova, G. V.; Ziger, E. A.; Koshkin, V. M.; Struchkov, Y. T.; Shklover, V. E. *Russ. J. Inorg. Chem.* **1988**, *33*, 977.
(28) Lazarini, F. *Acta Crystallogr.* **1977**, *B33*, 2961.
(29) Ishihara, H.; Watanabe, K.; Iwata, A.; Yamada, K.; Kinoshita, Y.; Okuda, T.; Krishnan, V. G.; Dou, S.; Weiss, A. *Z. Naturforsch.* **1992**, *47a*, 65.
(30) Mitzi, D. B. *J. Chem. Soc., Dalton Trans*., in press.
(31) See, for example: (a) Jóźków, J.; Jakubas, R.; Bator, G.; Zaleski, J.; Decressain, R. *J. Phys. Chem. Solids* **2000**, *61*, 887. (b) Jakubas, R.; Zaleski, J.; Kosturek, B.; Bator, G. *J. Phys.: Condens. Matter* **1999**, *11*, 4731. (c) Lazarini, F. *Acta Crystallogr.* **1977**, *B33*, 2686.
(32) Chabot, B.; Parthé, E. *Acta Crystallogr.* **1978**, *B34*, 645.
(33) Kawai, T.; Shimanuki, S. *Phys. Status Solidi B* **1993**, *177*, K43.

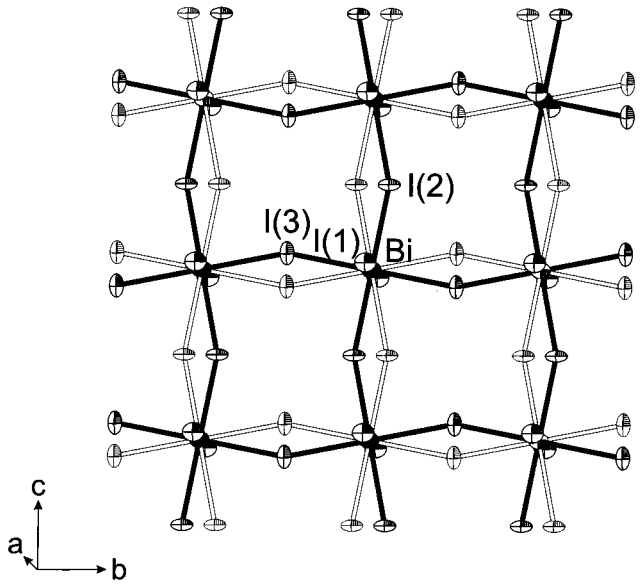

Figure 2. Bismuth(III) iodide framework in $(H_2AEQT)Bi_{2/3}I_4$ (*C*2/*m* cell). The bridging iodides within the perovskite sheets, I(2) and I(3), are distributed with half-occupancy over two symmetry-related sites, suggesting an unresolved superstructure or disorder. One configuration for the bismuth(III) iodide framework is represented with heavier lines and filled bonds. For clarity, the alternative configuration for the framework is represented with lighter lines and unfilled bonds. The thermal ellipsoids for the bismuth and iodine atoms are drawn at 50% probability.

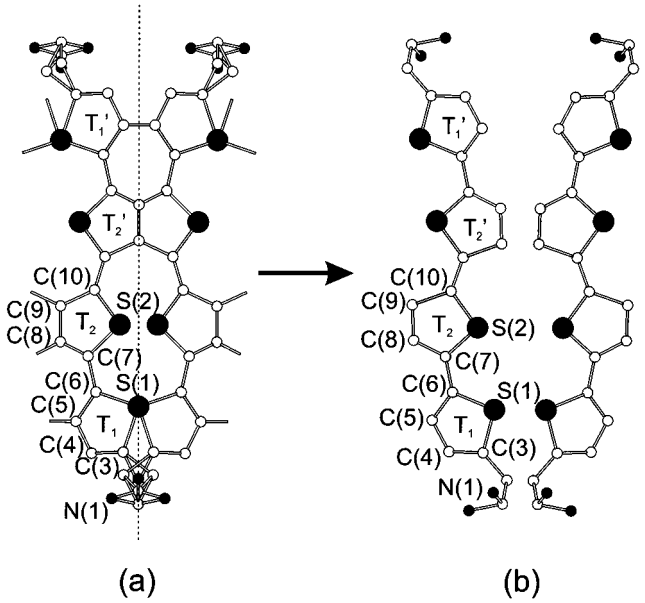

Figure 3. The doubly protonated 5,5‴-bis(aminoethyl)-2,2′:5′,2″:5″,2‴-quaterthiophene (AEQT) molecule in $(H_2AEQT)Bi_{2/3}I_4$ for (a) the *C*2/*m* subcell and (b) the *C*2/*c* cell models. For clarity, the atoms are represented as spheres with uniform sizes selected for each atom type. The mirror plane is marked with a dashed line in part a. In part b, the nitrogen atoms are disordered over two sites with equal occupancy.

In the current bismuth(III) and antimony(III) iodide structures, each metal cation vacancy creates a local concentration of negative charge. The creation of a substantial number of randomly positioned vacancies should be energetically unfavorable, unless some additional aspect of the system can help to offset the energy deficit. It is therefore interesting to consider the potential role played by the AEQT cation layer in stabilizing the unusual metal-deficient ⟨100⟩-oriented perovskites layers.

Oligothiophene Conformation and Ordering. The conformation of the protonated 5,5‴-bis(aminoethyl)-2,2′:5′,2″:5″,2‴-quaterthiophene molecule in $(H_2AEQT)Bi_{2/3}I_4$ is shown in Figure 3, with the molecular conformation of the antimony(III) analogue being essentially identical. Each quaterthiophene oligomer can be fully described by two independent thiophene rings, T_1{S(1), C(3), C(4), C(5), C(6)} and T_2{S(2), C(7), C(8), C(9), C(10)}. The other half of the quaterthiophene oligomer is generated by symmetry, yielding the rings T_1'{S(1)′, C(3)′, C(4)′, C(5)′, C(6)′} and T_2'{S(2)′, C(7)′, C(8)′, C(9)′, C(10)′}. In the subcell (*C*2/*m*) model, disordering of each organic cation across a mirror plane corresponds to the superposition of two-half-occupied quaterthiophene configurations (Figure 3a). Analogous perovskites cells have been reported for (2-phenethylammonium)$_2PbI_4$,[3] (2-naphthylmethylammonium)$_2PbCl_4$,[34] and (2-anthrylmethylammonium)$_2PbCl_4$,[35] each of which exhibits the same type of organic cation disordering or (perhaps more likely) unresolved superstructure. Note that by doubling the cell along the *c* axis and adopting the *C*2/*c* cell, as in $(H_2AEQT)PbX_4$ (X = Br, I), the two conjoined orientations of the AEQT quaterthiophene moiety become separated (Figure 3b) and alternate down the *c* axis of the structure. In fact, the disordered quaterthiophene layer of the *C*2/*m* cell is essentially a superposition of two symmetry-related configurations, each of which corresponds to the non-disordered *C*2/*c* cell quaterthiophene layer structure. For convenience, the discussion of the organic layer given below is based on the *C*2/*c* refinement. The analysis from the *C*2/*m* cell is essentially identical, after taking into consideration the disordering between the two possible organic layer configurations.

The AEQT bond lengths and angles in $(H_2AEQT)Bi_{2/3}I_4$ and $(H_2AEQT)Sb_{2/3}I_4$ are similar to those observed in the lead(II) halide based systems.[11] Each thiophene ring is essentially planar, with a dihedral angle between the planes defined by the thiophene rings, T_1 and T_2 (or T_1' and T_2'), of approximately 6(1)° for both the bismuth and antimony systems. While the all-anti (or all-trans) backbone conformation is most typical among oligothiophenes (e.g., α-quaterthiophene and other unsubstituted oligothiophenes),[36−38] the syn-anti-syn conformation is adopted in the bismuth(III) and antimony(III) perovskites (Figure 3), as is also the case in the related system, $(H_2AEQT)PbX_4$.[11] Several other examples of nearly planar syn-anti-syn conformation have also recently appeared, including 5,5‴-bis-[(2,2,5,5-tetramethyl-1-aza-2,5-disila-1-cyclopentyl)ethyl]-2,2′:5′,2″:5″,2‴-quaterthiophene.[38] The quaterthiophene oligomers pack into the layered perovskite framework such that the oligomers are substantially tilted relative to the perovskite sheet normal (Figure 1). The least-squares best plane through the quaterthiophene section of the AEQT molecule (averaging over the slight misorientation of the planes defined by the T_1 and T_2 rings) forms a dihedral angle of 40.0(5)° [38.6(4)°] with respect to the plane containing the Bi [Sb], I(2), and I(3) atoms (i.e., the plane of the perovskite sheets). These angles are comparable with the corresponding angles in $(H_2AEQT)PbI_4$ (40.2°) and $(H_2AEQT)PbBr_4$ (44.5°).[11]

(34) Braun, M.; Frey, W. *Z. Kristallogr.—New Cryst. Struct.* **1999**, *214*, 333.
(35) Braun, M.; Frey, W. *Z. Kristallogr.—New Cryst. Struct.* **1999**, *214*, 335.
(36) Siegrist, T.; Kloc, C.; Laudise, R. A.; Katz, H. E.; Haddon, R. C. *Adv. Mater.* **1998**, *10*, 379.
(37) Barone, V.; Lelj, F.; Russo, N.; Toscano, M. *J. Chem. Soc., Perkin Trans. 2* **1986**, 907.
(38) Muguruma, H.; Kobiro, K.; Hotta, S. *Chem. Mater.* **1998**, *10*, 1459.

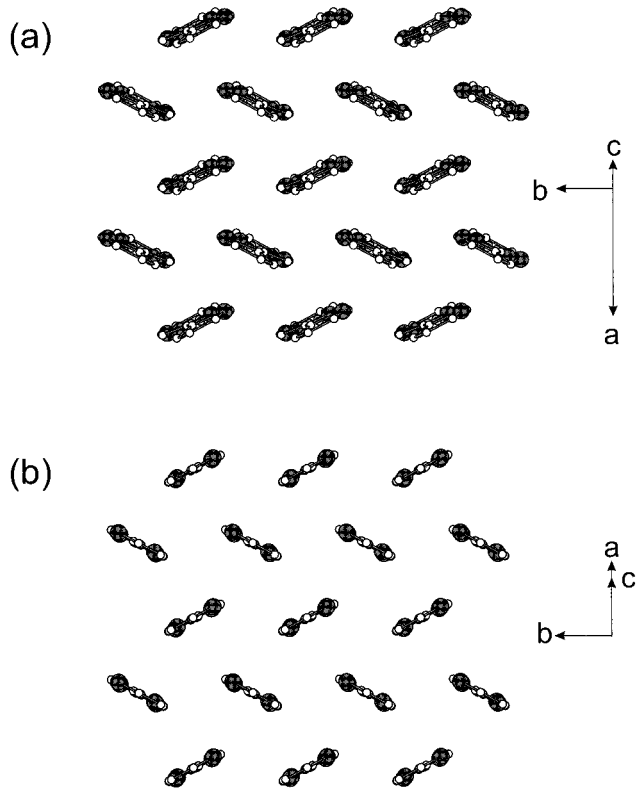

Figure 4. (a) View down the long molecular axis of one layer of AEQT cations in the $(H_2AEQT)Bi_{2/3}I_4$ structure (*C*2/*c* cell). For clarity, only the quaterthiophene component of the AEQT molecule is drawn, clearly demonstrating the herringbone arrangement of the quaterthiophene units in the structure. The analogous view for the antimony(III) system, $(H_2AEQT)Sb_{2/3}I_4$, is essentially indistinguishable from the figure for the bismuth(III) compound. In part b, a similar view for one layer of quaterthiophene molecules in crystalline α-quaterthiophene[36] is shown for comparison.

Viewing down the length of the quaterthiophene molecules, the oligomers in $(H_2AEQT)Bi_{2/3}I_4$ and $(H_2AEQT)Sb_{2/3}I_4$ adopt a herringbone arrangement, similar to that found in purely organic crystals and films of the various oligothiophenes (Figure 4).[39−42] In fact, the AEQT layer structure in $(H_2AEQT)Bi_{2/3}I_4$ [also in $(H_2AEQT)Sb_{2/3}I_4$, $(H_2AEQT)PbI_4$, or $(H_2AEQT)PbBr_4$], viewed down the long axis of the quaterthiophene moiety (Figure 4a), can virtually be superimposed on a layer from α-quaterthiophene viewed similarly (Figure 4b), despite the very different environment in which the quaterthiophene moiety is held (i.e., the inorganic framework) and the different molecular conformation (i.e., syn-anti-syn versus all-anti). The herringbone angle for the bismuth(III) system is approximately 50.0°, similar to that observed in $(H_2AEQT)PbBr_4$ (51.2°) and α-quaterthiophene (55.7°).

The herringbone arrangement of the quaterthiophene moieties is common among other aromatic organic molecules (e.g., naphthalene,[43] anthracene,[44] biphenyl,[45] and quaterphenyl[46]) and can be explained in terms of edge-to-face (tilted-T) aromatic interactions.[40,47−51] These interactions arise as a result of electrostatic and London dispersion effects (i.e., van der Waals interactions)[48,49] and are now believed to play an important role in protein folding[50] and molecular recognition in aromatic systems.[51] The edge-to-face interaction energy for a single benzene dimer in the gas phase is approximately −2 kcal/mol,[49] similar in magnitude to a weak hydrogen bond (a similar order of magnitude interaction would also be expected for two thiophene rings). Note, however, that for longer oligomers, consisting of a rigid network of multiple aromatic components, the effects of these interactions add up and can therefore have a more substantial structure-directing influence on the resulting system. For example, in the $NC(T_n)CN$ ($n = 3-6$) series, where T_n denotes an oligothiophene moiety with "*n*" units, competing forces drive the ordering of the oligothiophene units.[40] For shorter oligothiophenes ($n = 3-5$), the intermolecular CN···H interactions induce the molecules to adopt a slipped π-stack structure. In contrast, for a longer oligothiophene ($n = 6$), the edge-to-face interactions dominate, and the structure adopts the more traditional herringbone arrangement.

For the rigid quaterthiophene moiety (e.g., AEQT), the effect of the edge-to-face interactions is similarly expected to be important during both solution crystal growth and evaporative thin-film deposition. One possible mechanism for the stabilization of the metal-deficient ⟨100⟩-oriented perovskite structures therefore involves the preferential formation of two-dimensional layers of AEQT, stabilized by the edge-to-face interactions (as well as other interactions leading to the stable organic cation layers), which in turn template the formation of the unusual metal-deficient two-dimensional anions rather than more typical isolated or one-dimensional species with fully occupied metal sites.

Conclusion

Single-layer ⟨100⟩-oriented hybrid perovskites generally consist of MX_4^{2-} divalent metal halide inorganic frameworks separated by layers of organic cations. In this study, the layered perovskite family has been extended to include the members $(H_2AEQT)M_{2/3}I_4$ ($M = Bi^{3+}$, Sb^{3+}), where the higher-valent metal halide inorganic sheets are stabilized by vacancy formation on the metal site and by an organic cation that can template the formation of two-dimensional perovskite layers. The formula for the inorganic sheets can also be written $(M^{3+})_{2/3}V_{1/3}X_4^{2-}$ ($X = Cl$, Br, I), where V represents a vacancy (usually left out of the formula). Given an appropriate organic cation layer, it is likely that the new hybrid perovskite family can be further generalized to include other higher-valent metal halide inorganic frameworks. For tetravalent metals (e.g., Sn^{4+}, Te^{4+}, Hf^{4+}) the inorganic anion layer would be expressed as $(M^{4+})_{1/2}V_{1/2}X_4^{2-}$, while for pentavalent metals (e.g., Nb^{5+}, Ta^{5+}, Mo^{5+}) it would be $(M^{5+})_{2/5}V_{3/5}X_4^{2-}$. In general, for an *n*-valent metal, the $(M^{n+})_{2/n}V_{(n-2)/n}X_4^{2-}$ inorganic framework contains just enough vacancies to provide a +2 average charge on the metal site. Note that, for sufficiently large *n*, the concentration of vacancies might eventually become too high for the perovskite structure to be energetically favorable.

(39) Antolini, L.; Horowitz, G.; Kouki, F.; Garnier, F. *Adv. Mater.* **1998**, *10*, 382.
(40) Barclay, T. M.; Cordes, A. W.; MacKinnon, C. D.; Oakley, R. T.; Reed, R. W. *Chem. Mater.* **1997**, *9*, 981.
(41) Hotta, S.; Waragai, K. *Adv. Mater.* **1993**, *5*, 896.
(42) Porzio, W.; Destri, S.; Mascherpa, M.; Brückner, S. *Acta Polym.* **1993**, *44*, 266.
(43) Brock, C. P.; Dunitz, J. D. *Acta Crystallogr.* **1982**, *38B*, 2218.
(44) Brock, C. P.; Dunitz, J. D. *Acta Crystallogr.* **1990**, *46B*, 795.
(45) Hargreaves, A.; Rizvi, S. *Acta Crystallogr.* **1962**, *15*, 365.
(46) Delugeard, Y.; Desuche, J.; Baudour, J. L. *Acta Crystallogr.* **1976**, *B32*, 702.
(47) Hunter, C. A.; Sanders, J. K. M. *J. Am. Chem. Soc.* **1990**, *112*, 5525.
(48) Paliwal, S.; Geib, S.; Wilcox, C. S. *J. Am. Chem. Soc.* **1994**, *116*, 6, 4497.
(49) Jorgensen, W. L.; Severance, D. L. J. *J. Am. Chem. Soc.* **1990**, *112*, 4768.
(50) Burley, S. K.; Petsko, G. A. *Science* **1985**, *229*, 23.
(51) Seel, C.; Vögtle, F. *Angew. Chem., Int. Ed. Engl.* **1992**, *31*, 528.

Since there is no evidence of long-range vacancy ordering from the current single-crystal X-ray data, the metal-site vacancies are considered randomly distributed. The metal sites within the $(M^{n+})_{2/n}V_{(n-2)/n}X_4^{2-}$ network are essentially arranged in a two-dimensional square lattice and each site is occupied with probability $p = 2/n$. Numerical calculations for an infinite two-dimensional square lattice predict a percolation threshold at $p_c = 0.59$.[52] Consequently, the title $n = 3$ systems are notable because they are the only members of the new family of metal-deficient perovskites (i.e., with $n > 2$) in which infinite clusters of corner-sharing metal halide octahedra are predicted to extend entirely across the inorganic layers. The current Bi^{3+} and Sb^{3+} systems are therefore interesting with respect to the electronic properties of the inorganic sheets. Note that the organic component of the hybrid structures can also play an important role in the optical and electrical properties. The study of crystalline oligothiophene and other oligomer layers has been of recent interest in terms of both fundamental electrical transport studies and the potential application of these materials in thin-film transistor channel layers.[53−55] The use of the inorganic framework to constrain or control the packing and ordering of the oligomer layers in the hybrid structures has also been discussed.[11]

While the creation of metal-deficient perovskite sheets through the incorporation of higher-valent metals is, at least in principle, very straightforward, as vacancies are introduced on the metal site of the inorganic layers, there should be a driving force toward the formation of other non-perovskite structures (i.e., ones with essentially no metal-site vacancies). For example, in bismuth(III) halide systems with simple alkyldiammonium cations, the layered organic−inorganic perovskite structure has so far not been formed, despite the occurrence of numerous examples of layered perovskites based on these same organic cations for divalent metal halides.[22] In order to stabilize the layered perovskite framework with the higher-valent metals, it is therefore important to choose an organic countercation that will facilitate or template the formation of the characteristic inorganic layers of corner-sharing metal halide octahedra.

The stabilization provided by the organic cation layers in the title $(H_2AEQT)M_{2/3}I_4$ ($M = Bi^{3+}$, Sb^{3+}) compounds presumably derives from both the rigid, rodlike nature of the AEQT molecule and the edge-to-face interactions provided by the four aromatic entities of each molecule. Given these constraints, it is likely that numerous other organic cations can also be used to stabilize the higher-valence metal-deficient perovskite frameworks exhibited in the $(H_2AEQT)M_{2/3}I_4$ ($M = Bi^{3+}$, Sb^{3+}) systems. In addition to various length oligothiophene derivatives, analogous oligophenylene derivatives are likely to be suitable. Other organic cations based on the oligocene (e.g., naphthalene, anthracene, tetracene, pentacene) series might also be appropriate to consider, since these rigid molecules are subject to substantial edge-to-face interactions and regularly align themselves into herringbone-structured layers. Analysis of hybrids containing these alternative organic cations, as well as other related systems, will further elucidate the templating mechanism that is suggested by the current structures.

Supporting Information Available: Tables providing a full listing of experimental and crystallographic data (Table S1), anisotropic temperature factors for $(H_2AEQT)Bi_{2/3}I_4$ (Table S2) and $(H_2AEQT)Sb_{2/3}I_4$ (Table S3), and bond distances and angles for $(H_2AEQT)Bi_{2/3}I_4$ (Table S4) and $(H_2AEQT)Sb_{2/3}I_4$ (Table S5). In addition to the data listed above for the *C*2/*m* subcell refinement, similar data for the *C*2/*c* cell refinement are also given (Tables S6−S12) for comparison. This material is available free of charge via the Internet at http://pubs.acs.org.

IC000794I

(52) Stauffer, D. *Phys. Rep.* **1979**, *54*, 1.
(53) Garnier, F. *Chem. Phys.* **1998**, *227*, 253.
(54) Servet, B.; Horowitz, G.; Ries, S.; Lagorsse, O.; Alnot, P.; Yassar, A.; Deloffre, F.; Srivastava, P.; Hajlaoui, R.; Lang, P.; Garnier, F. *Chem. Mater.* **1994**, *6*, 1809.
(55) Dimitrakopoulos, C. D.; Furman, B. K.; Graham, T.; Hegde, S.; Purushothaman, S. *Synth. Met.* **1998**, *92*, 47.